JOURNAL OF SOLID STATE CHEMISTRY 58, 383–388 (1985)

Structure and Microstructure of the Metastable B Phase ($NiAl_{10}O_{16}$)

I. Preparation and Structural Study by X-Ray Diffraction

P. BASSOUL AND J. C. GILLES

Laboratoire de Chimie du Solide Minéral–UA 450, ESPCI 10 rue Vauquelin, 75231 Paris Cedex 05, France

Received May 25, 1984; in revised form December 26, 1984

The B phase of composition $NiAl_{10}O_{16}$ is one of the metastable phases found in the Al_2O_3–NiO system. Twinned crystals of B were prepared by annealing samples at 1150°C. Indexing the crystal diffraction patterns with 12 twin variants was done. A structural model belonging to the space group $P2_1/b$ is proposed. The B phase has a periodic antiphase boundary (PAPB) structure based on the (100) spinel planes with an antiphase vector $\mathbf{R} = \frac{1}{4}[1\bar{1}0]$. Moreover this structure is slightly modified by introducing periodic steps on PAPB planes. These steps give rise to a particular order of cation vacancies. © 1985 Academic Press, Inc.

1. Introduction

The spinel phase $NiAl_2O_4$ has an extended solid solution domain in the Al_2O_3–NiO system at high temperatures (Fig. 1). Many binary systems such as Al_2O_3–MgO, Al_2O_3–AlN, Al_2O_3–Li_2O, or Ga_2O_3–MgO have solid solution domains with spinel structure. The structure of nonstoichiometric spinel phases (γ) has been explained by the formation of disordered cation vacancies when the alumina (or gallia) ratio is increased (1 to 4). The formula for nickel aluminate solid solution is $Ni_{1-3x}\square_x Al_{2+2x}O_4$ ($\square$: cation vacancy). Another property of these systems is that metastable phases can be prepared by melting the oxide powder mixture. They crystallize in the quentched melts or precipitate in the nonstoichiometric spinel matrix when the samples are annealed. Metastable phases disappear and the stable phases (γ + α-Al_2O_3 or β-Ga_2O_3) precipitate when a longer annealing time is used.

The metastable phase structures are characterized by their cubic pseudosymmetry. Their precipitation from spinel solid solution gives rise to twinned crystals on a small scale with a great number of twin variants. These characteristics were revealed with the first attempts to determine the φ phase structure in the Al_2O_3–MgO system made by Jagodzinski (*1*).

We shall first recall previous investigations on metastable phases in the Al_2O_3–NiO system. Then we describe X-ray diffraction patterns of the B phase twinned crystals and we propose a new type of periodic antiphase boundary (PAPB) structural model built from the spinel structure. A following paper (Part II) will be concerned with the investigation of the B phase microstructure by electron microscopy.

2. Metastable Phases in the Al_2O_3–NiO System

Several metastable phases have been prepared in the Al_2O_3–NiO system (Fig. 1) (*2–4*). All the metastable phases have a slightly

0022-4596/85 $3.00

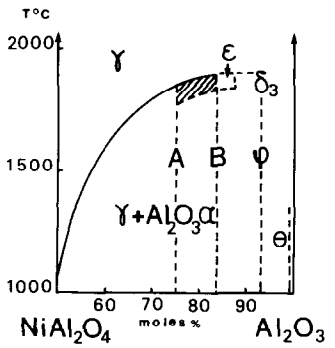

FIG. 1. Phase diagram for the $NiAl_2O_4$–Al_2O_3 system. Only γ and α-Al_2O_3 are stable phases.

distorted compact cubic oxygen array. The main differences in their structure are due to the cation distribution in the octahedral and tetrahedral interstices of this array. The φ and θ phases, respectively, are isomorphic with the φ phase in the Al_2O_3–MgO system (*1*) and with β-Ga_2O_3 (*4, 5*). All the other metastable phase structures have been described with PAPB structures built from the spinel structure. ε_{Ni} is composed with one PAPB system on $(310)_S$ spinel planes (*6, 7*). Phase A is composed of two PAPB systems on $\{311\}_S$ (*8, 9*). The structure of δ_3 can be related to the δ phase PAPB structure on $(100)_S$ planes (*10*). The structure of the high-temperature phases (hatched area in Fig. 1) are intermediate between A and ε structures. Their PAPBs are not strictly periodic; they give rise to diffuse streaks between satellite reflexions on diffraction patterns (*9*). PAPB structural models appear to be pertinent models to determine the cation distribution in the structures of these metastable phases.

3. Preparation

The B phase composition given by Colin (*4*) was $4.5Al_2O_3 \cdot NiO$, but his investigations were based on powder diagrams only. Single crystal oscillation methods show that crystals of this composition contain two syntactic A and B phases. Pure B crystals could be prepared only by melting and annealing samples of composition $5Al_2O_3 \cdot NiO$. When the oxide powder mixture is melted in an arc image furnace and quenched into water, the first phase obtained is ε_{Ni}. If samples are air-cooled, a small quantity of ε_{Ni} is then transformed into B phase. Finally ε_{Ni} is completely transformed into B phase after an annealing time of 90 hr at 1150°C. For annealing times longer than 150 hr at this temperature the stable α-Al_2O_3 phase precipitates.

4. Diffraction Patterns of Twinned Crystals

The powder diagram of the B phase shows strong diffraction lines close to those of the spinel structure plus a great number of weaker lines. Strong lines were indexed on a monoclinic pseudocubic cell having the following parameters:

$$a'_c = 7.98\ \text{Å}, \quad b'_c = 7.88\text{Å}, \quad c'_c = 7.95\ \text{Å} \quad \gamma'_c = 91.1°.$$

The Weissenberg and precession photographs exhibit cubic point symmetry. All the spots on the films correspond to reflection clusters (Fig. 2). The fine structure of these spots can be explained by superimposition of the reflections coming from 12 monoclinic twin variants. Each twin variant unit cell is precisely twice the pseudocubic cell:[1]

$$a_m = a'_c, \quad b_m = 2b'_c, \quad c_m = c'_c, \quad \gamma_m = \gamma'_c.$$

In order to determine the B space group it was necessary to know precisely each twin variant contribution to the fine structure of spots. A calculation of the exact reflection

[1] The unit cell proposed by Colin for the B phase has the same pseudocubic distortion as ours, but a different double parameter ($c_m = 2c'$). We think that the true unit cell cannot be determined by powder diagrams only, as was done by Colin; single crystal patterns are also necessary.

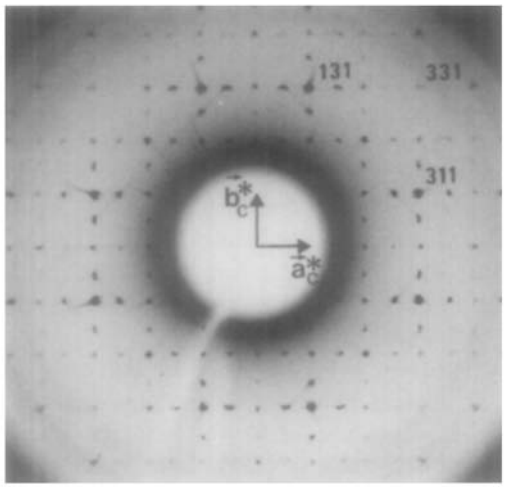

FIG. 2. Precession diffraction photograph of a twinned crystal with 12 twin variants (λ Cu$K\alpha$). $(001)^*_c$ plane, layer 1. Indices are those of fundamental spinel spots referring to the cubic cell.

coordinates of each variant, referred to the same cubic lattice ($\mathbf{a}_c$, $\mathbf{b}_c$, $\mathbf{c}_c$) was made. The distortion of the direct space pseudocubic lattice could be described by a matrix A, if twin variant number 1 (see Table I) is taken as the reference variant:

$$A = \begin{bmatrix} 1+\alpha & \omega & 0 \\ 0 & 1+\beta & 0 \\ 0 & 0 & 1 \end{bmatrix}$$

$$\alpha = \frac{a'_c - a_c}{a_c}, \qquad \beta = \frac{b'_c \sin \gamma'_c - a_c}{a_c},$$

$$\omega = \frac{b'_c \cos \gamma'_c}{a_c},$$

with orientation relationships $\mathbf{a}_c \| \mathbf{a}'_i$, $\mathbf{c}_c \| \mathbf{c}'_i$, and $|\mathbf{c}_c| = |\mathbf{c}'_i|$. Matrix A relates the components of vectors $\mathbf{x}'_i$ of the distorted lattice to those of $\mathbf{x}_c$: $\mathbf{x}'_i = A\mathbf{x}_c$. Let us now consider a twin variant i and its symmetry operation described by the matrix R_i. The $\mathbf{x}'_i$ vector of this variant, which is close to $\mathbf{x}_c$, is related to $\mathbf{x}_c$ by the relation

$$\mathbf{x}'_i = R_i A R_i^{-1} \mathbf{x}_c. \qquad (1)$$

The corresponding relation in reciprocal space is

TABLE I

TWIN VARIANTS PRODUCED BY A SET OF 12 TWIN OPERATIONS

	e	$m_{(100)_c}$	$m_{(110)_c}$	$C^1_{4[001]_c}$	Binary axis direction
e	1 $[010]^*_c$[a]	2 $[010]^*_c$	3 $[100]^*_c$	4 $[100]^*_c$	$[001]_c$
$C^1_{3[111]}$	1′ $[001]^*_c$	2′ $[001]^*_c$	3′ $[010]^*_c$	4′ $[010]^*_c$	$[100]_c$
$C^2_{3[111]}$	1″ $[100]^*_c$	2″ $[100]^*_c$	3″ $[001]^*_c$	4″ $[001]^*_c$	$[010]_c$

[a] Modulation direction of each twin variant.

$$\mathbf{x}'^*_i = R_i A^{-1} R_i^{-1} \mathbf{x}^*_c. \qquad (2)$$

Relation (2) gives the exact coordinates of the 12 twin variant reflections which can possibly contribute to the fine structure of the spot described by $\mathbf{x}^*_c$. By applying formula (2), the fine structure of the spots was determined and reflection of each twin variant was indexed. Figure 3 gives the contribution of the 12 twin variants to the satellite reflections related to the spots corresponding to spinel structure. The details of 131_c fine structure for the fundamental and the satellite reflections are given as an example in Fig. 4.

For one twin variant, the inferred diffraction pattern contains three types of reflections:

—Fundamental reflections, which are very strong and close to reciprocal nodes of a spinel structure. They are described by the vectors

$$\mathbf{V}^* = h_c \mathbf{a}'^*_c + k_c \mathbf{b}'^*_c + l_c \mathbf{c}'^*_c \quad \text{with } h_c - k_c = 4n.$$

—Satellite reflections, along the $[010]^*_c$ direction, corresponding to the absent fundamental reflections. They are described by the vectors

$$\mathbf{V}^* = h_c \mathbf{a}'^*_c + k_c \mathbf{b}'^*_c + l_c \mathbf{c}'^*_c \pm m \frac{\mathbf{b}'^*_c}{2},$$

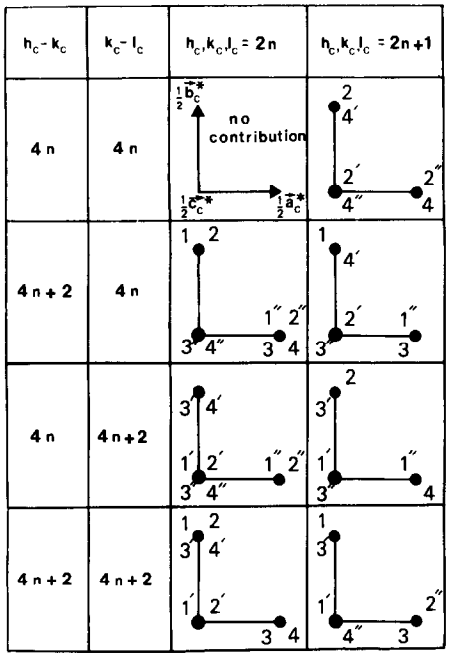

FIG. 3. Satellite reflexions surrounding a fundamental spinel spot. $h_ck_cl_c$ indices refer to the cubic unit cell. For twin variant number see Table I.

with $h_c - k_c = 4n + 2$ and m odd.

—Additional reflections that cannot be described as fundamentals or satellites are at the other nodes of the lattice

$$\mathbf{a}_m^* = \mathbf{a}_c'^*, \qquad \mathbf{b}_m^* = \frac{\mathbf{b}_c'^*}{2}, \qquad \mathbf{c}_m^* = \mathbf{c}_c'^*.$$

The satellite reflections along the $[010]_c^*$ direction and the extinction of corresponding fundamentals are characteristic of a PAPB structure on $(010)_c$ spinel planes with an antiphase vector $\mathbf{R} = \frac{1}{4}[1\bar{1}0]_c$. We will see in the next paragraph that this PAPB structure must be slightly modified to introduce the additional reflections.

5. Structural Model

Previous studies of PAPB structures built on spinel structure (*6–10*) have shown that the main features of the diffraction patterns are explained with the distribution of cations in these structures. PAPBs introduce a new arrangement in the tetrahedral and octahedral interstices of the distorted compact cubic oxygen array. Antiphase vectors are vectors of the oxygen sublattice and they affect the cation distribution only. Thus, to build a structural model for the B phase, we leave aside the monoclinic distortion and take the cation sites in an idealized compact cubic oxygen array as a good approximation.

Figure 5 shows a PAPB structure on $(010)_c$ spinel planes with spacing d_{010_c} and an antiphase vector $\mathbf{R} = \frac{1}{4}[1\bar{1}0]_c$. It can be seen that, on each PAPB plane, each tetrahedral site shares a face with one octahedral site. Two sites sharing a face cannot be occupied simultaneously (*10*). This rule yields the composition $5Al_2O_3 \cdot NiO$, which has been found for the B phase. When vacancies are located on the octahedral sites sharing a face or on the tetrahedral ones, the space group found is $B2/b$. These two models are in agreement with the strong satellites reflections and the extinction of

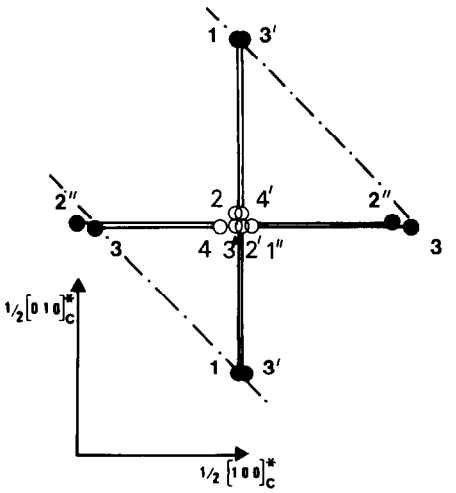

FIG. 4. Schematic representation of fundamental and satellite reflections of 131_c observed on the precession diffraction photograph (Fig. 2): satellites reflections of order 1 (●); fundamental reflections (○). Diffuse lines are represented by mixed lines. For twin variant number see Table I.

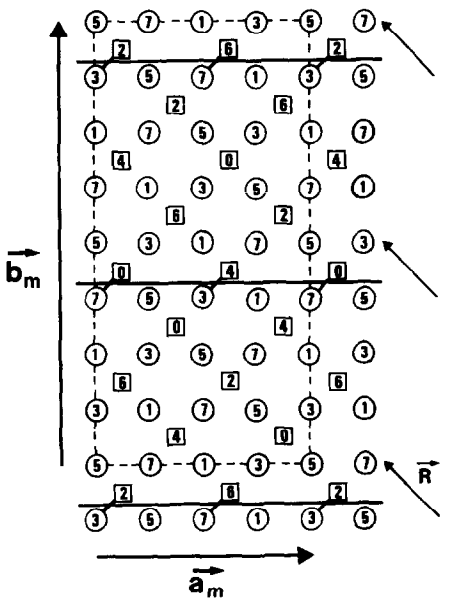

FIG. 5. PAPB structural model, $(001)_c$ projection of cations. APB plane $(010)_c$. Antiphase vector $\mathbf{R} = \frac{1}{4}[1\bar{1}0]_c$, octahedral sites (○), tetrahedral sites (□). The heights of cations are given as multiples of $c_c/8$. Octahedral and tetrahedral sites with a common face are connected by a line.

the corresponding fundamentals, but they do not fit with the observed additional reflections.

In order to account for the additional reflections, a P lattice should be considered instead of B lattice. This will be done by a slight modification of the cation distribution near the PAPB plane. Steps are introduced in the PAPB plane in order to obtain what we call a "crenellated PAPB." Such steps will correspond to one cationic plane and their length will be $\frac{1}{2}[100]_c$. Figure 6 shows a structural model of this type. This cation rearrangement will maintain the same number of face-sharing sites, as can be seen in Figs. 5 and 6. The different structural models built with "crenellated PAPB" differ by the relative position of steps on two successives PAPBs. A systematic investigation of these models lead to three types of structures with $P2_1/b$, $P2/b$, $P2/n$ space groups. From the observation of $(h_m k_m 0)$ reflections with $h_m + k_m = 2n + 1$, $P2/n$ can be excluded. Calculations corresponding to the structural model with space group $P2/b$ shows that calculated $(00l_m)$ reflections with $l_m = 2n + 1$ have quite the same intensity as the $(00l_m)$ reflections with $l_m = 2n$. Since reflections with $l_m = 2n + 1$ are not observed, only the structural model with space group $P2_1/b$ (Fig. 6) will be consistent with the diffraction patterns. There is a good qualitative agreement between calculated $|F_{hkl}|^2$ (Fig. 7) and the observed reflection intensities when a statistical distribution of aluminium and nickel ions on nonvacant octahedral sites of this model is used. Nickel ions could be ordered on some octahedral sites without changing the space group, (a) or (b) sites of Fig. 6, for example. But, if the occupied sites are completely determined by the model, ordering between nickel and aluminium ions cannot be tested since its effect on the $|F_{hkl}|^2$ values is too small.

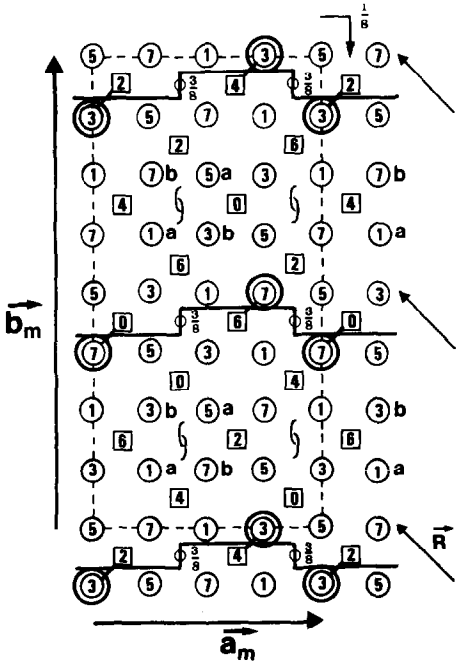

FIG. 6. Structural model of the B phase with space group $P2_1/b$ (see caption of Fig. 5). Vacant octahedral sites (◎).

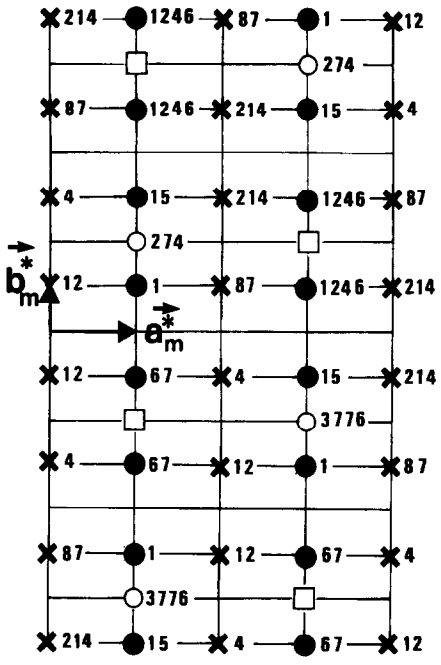

FIG. 7. Calculated values of $F^2 = (F_{hkl})^2/(F_{000})^2 \times 10^4$ from the structural model of Fig. 6. $(001)_m^*$, layer 1. Reflections: present fundamentals (○); absent fundamentals (□); satellites (●); additionals (×). Reflections with $F^2 < 1$ are not indicated.

6. Conclusion

The cubic pseudosymmetry and the multiple twinning (12 twin variants) encountered in the monoclinic B phase ($NiAl_{10}O_{16}$) hinders its structure determination by conventional methods using measured intensities. Nevertheless, a precise indexing of the diffraction patterns of twinned crystal shows that phase B has a PAPB structure built on the spinel structure. A particular distribution of cations and vacancies, which has been described as periodic "crenellated PAPBs," appears in this structure. Vacancies are paired at two close octahedral sites of the spinel structure in the vicinity of PAPB planes. In a following paper (Part II) it will be shown that the microstructural characteristics observed by transmission electron microscopy can be explained in terms of the proposed structural model.

References

1. H. JAGODZINSKI, *Z. Kristallogr.* **109,** 388 (1957).
2. H. SCHMALZRIED, *Z. Phys. Chem.* **28,** 203 (1961).
3. A. M. LEJUS, *Rev. Hautes Temp. Refract.* **1,** 53 (1964).
4. F. COLIN, *Rev. Hautes Temp. Refract.* **5,** 267 (1968).
5. S. GELLER, *J. Chem. Phys.* **33,** 676 (1960).
6. P. BASSOUL, A. LEFEBVRE, AND J. C. GILLES, *Mater. Res. Bull.* **11,** 11 (1976).
7. P. BASSOUL, A. DUBON, A., LEFEBVRE, AND J. C. GILLES, *Phys. Status Solidi A* **34,** 125 (1976).
8. P. BASSOUL, A. LEFEBVRE, AND J. C. GILLES, *J. Solid State Chem.* **10,** 56 (1974).
9. P. BASSOUL, thesis, Paris (1979).
10. A. LEFEBVRE, *J. Appl. Crystallogr.* **8,** 235 (1975).